THE JOURNAL OF PHYSICAL CHEMISTRY A

Article

pubs.acs.org/JPCA

Dynamics of Excited States for Fluorescent Emitters with Hybridized Local and Charge-Transfer Excited State in Solid Phase: A QM/MM Study

Jianzhong Fan, Lei Cai, Lili Lin,* and Chuan-Kui Wang*

Shandong Province Key Laboratory of Medical Physics and Image Processing Technology, School of Physics and Electronics, Shandong Normal University, 250014 Jinan, China

Supporting Information

ABSTRACT: The highly efficient organic light-emitting diodes (OLEDS) based on fluorescent emitters with hybridized local and charge-transfer (HLCT) excited state have attracted great attention recently. The excited-state dynamics of the fluorescent molecule with consideration of molecular interaction are studied using the hybrid quantum mechanics/molecular mechanics method. The results show that, in solid state, the internal conversion rate (K_{IC}) between the first singlet excited state (S1) and the ground state (S0) is smaller than the fluorescent rate (K_r), while in gas phase K_{IC} is much larger than K_r. By analyzing the Huang−Rhys (HR) factor and reorganization energy (λ), we find that these two parameters in solid state are much smaller than those in gas phase due to the suppression of the vibration modes in low-frequency regions (<200 cm^{-1}) related with dihedral angles between donor and acceptor groups. This is further demonstrated by the geometrical analysis that variation of the dihedral angle between geometries of S1 and S0 is smaller in solid state than that in gas phase. Moreover, combining the dynamics of the excited states and the adiabatic energy structures calculated in solid state, we illustrate the suggested "hot-exciton" mechanism of the HLCT emitters in OLEDs. Our work presents a rational explanation for the experimental results and demonstrates the importance of molecular interaction for theoretical simulation of the working principle of OLEDs.

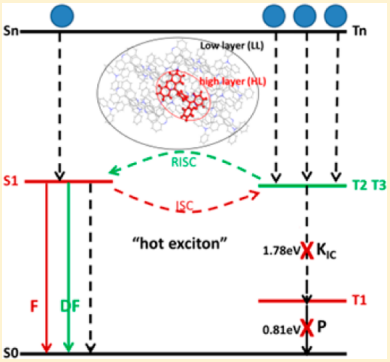

1. INTRODUCTION

Since the milestone work of Tang and VanSlyke in 1987, organic light-emitting diodes (OLEDs) have attracted great attention and become the research focus in organic electroluminescence both theoretically and experimentally.[1] According to the spin statistics, the singlet-to-triplet excitons formation ratio is expected to be 1:3 in the conventional fluorescent OLEDs.[2] Generally, only singlet excitons can be used, and the triplet excitons, which account for 75% of excitons, are wasted. The organometallic phosphorescent emitters have been developed by using the strong spin−orbit couplings of transition metals such as platinum and iridium.[3−5] Although the exciton utilization efficiency can be increased to nearly 100% using those phosphorescent materials, there are still many shortcomings needed to be solved such as the high cost and the lack of blue OLED material. Recently, Adachi's group proposed a new route to highly efficient fluorescent emitters by using thermally activated delayed fluorescence (TADF) phenomena.[6−10] One important consideration in the design of TADF molecules is that the energy gap between the first singlet excited state (S1) and the first triplet excited state (T1) should be small enough for efficient up-conversion. The general way to decrease the S1-T1 energy gap is connecting suitable donor (D) and acceptor (A) groups by a steric hindrance such as bulky, twist, or spirojunction, because such methods can effectively separate the spatial overlap between the highest occupied molecular orbital (HOMO) and lowest unoccupied molecular orbital (LUMO).[11] Meanwhile, one negative effect is generalized. The weak overlap of the transition orbitals involved in the charge transfer (CT) excited state will undesirably cause slow radiative rate and low photoluminescence efficiency. To overcome the defect of TADF molecules, some solutions have been proposed. Adachi's group found that the fluorescent rate can be enhanced by inserting π unit between D and A groups.[12] Ma's group proposed a new concept, that is, the hybridized local and charge transfer (HLCT) excited state.[13−15] The HLCT state possesses two combined and compatible characteristics: a large transition moment from a light-emitting (LE) state, which contributes to a high-efficiency radiation of fluorescence, and a weakly bound exciton from a CT state, which is responsible for the full exciton utilization. Therefore, the HLCT state provides a novel approach for the design of highly luminous D−A chromophores.

4-(Acridin-9-yl)-*N*,*N*-diphenylaniline (TPA-AC) molecule is a typical HLCT molecule designed by Ma's group (shown in Figure 1a).[15] Experimental result indicates that the exciton usage efficiency of TPA-AC molecule is 46%, which is higher than the normal singlet exciton proportion (25%). Thus, a "hot-exciton" mechanism (up-conversion process is from high triplet states

Received: September 29, 2016
Revised: November 7, 2016
Published: November 8, 2016

DOI: 10.1021/acs.jpca.6b09852
J. Phys. Chem. A 2016, 120, 9422−9430

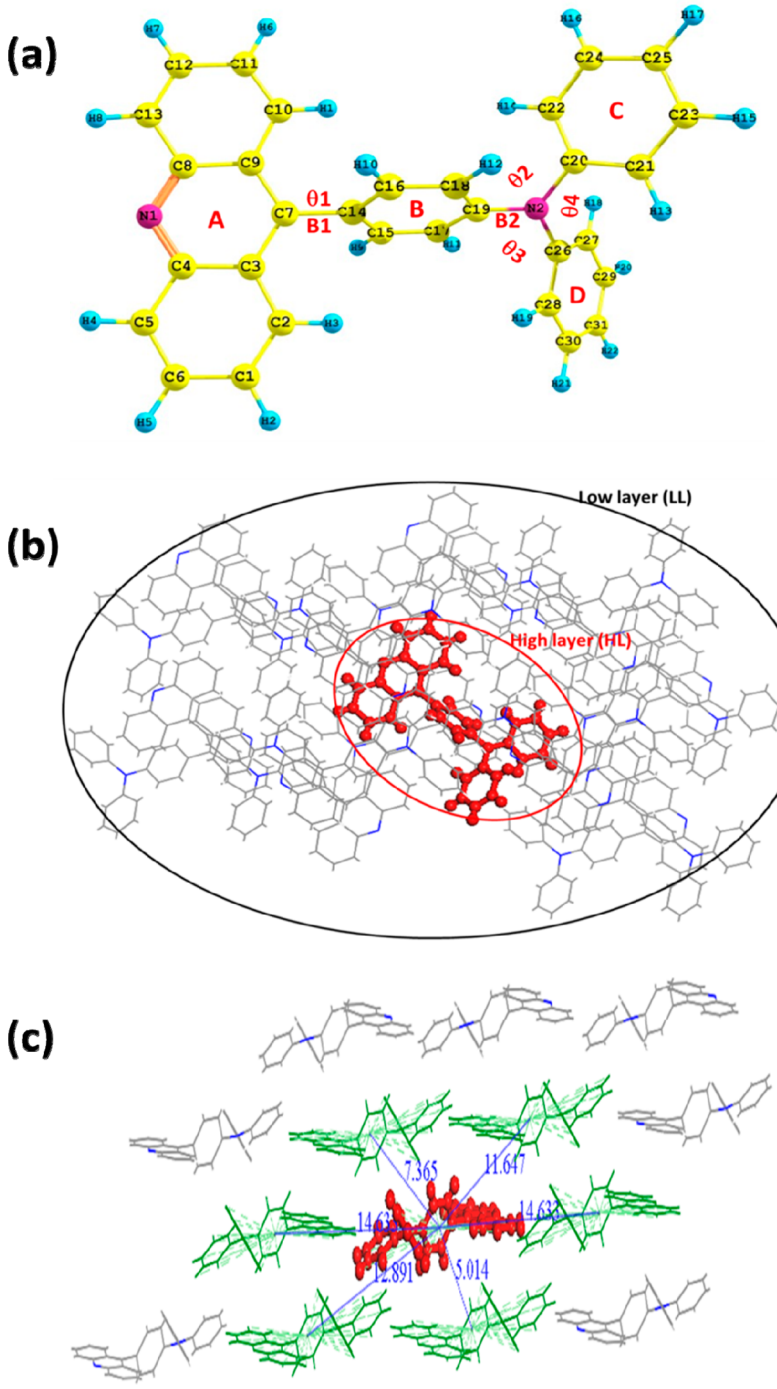

Figure 1. Chemical structure of the TPA-AC molecule in gas phase (a). ONIOM model: the centered TPA-AC molecule is treated as high layer, and the surrounding molecules are fixed as low layer (b). Close look at the packing structure with intermolecular distances labeled in angstroms (c).

(T2, T3, ...) rather than from T1) is proposed based on a quantum chemistry study of the TPA-AC molecule in gas phase.[15] As we find, the photoluminescence efficiency in solution is often different from that obtained in solid state.[15,16] Aggregation-caused quenching (ACQ) or aggregation-induced emission (AIE) have been observed in the solid state for fluorescent emitters.[16] Thus, the surroundings of the fluorescent emitters in solid state have important effect on their lighting-emitting properties, which have also been proven by some theoretical simulations.[17] In this paper, the excited-state dynamics of the TPA-AC molecule in solid state is studied by including the environment effect using the quantum mechanics/molecular mechanics (QM/MM) approach. Both the excited-states properties and the decay rates are analyzed in detail. Comparison with the calculation results in gas phase is also performed, which will give better understanding of the electroluminescent mechanism of the molecules in OLEDs.

2. THEORETICAL METHOD AND COMPUTATIONAL APPROACH

The molecular LE efficiency is determined by the competition between the radiative decay rate K_r and the nonradiative decay rate K_{nr} ($\eta_f = k_r + k_{nr}$, where η_f is the fluorescence efficiency). Either increasing the radiative rate or suppressing the non-

DOI: 10.1021/acs.jpca.6b09852
J. Phys. Chem. A 2016, 120, 9422−9430

radiative rate will result in high fluorescence efficiency. The nonradiative rate includes the internal conversion rate (K_{IC}) and the intersystem crossing rate (K_{ISC}). Therefore, theoretical calculations of radiative and nonradiative rates play an important role in predicting luminescent efficiencies.

The radiative decay rate can be computed by Einstein spontaneous emission rate equation, which is written as $k_r = \frac{f\Delta E_{fi}^2}{1.499\ \mathrm{cm}^{-2}\cdot\mathrm{s}}$, where f is oscillator strength without dimension, and ΔE_{fi} is in the unit of wavenumber (cm^{-1}).[18]

According to the Fermi's golden rule (FGR) and first-order perturbation theory, the nonradiative decay rate can be written as follows:

$$K_{NR} = \frac{2\pi}{\hbar^2}\sum_{u,v} P_{iv}|\hat{H}'_{fu,iv}|^2\delta(E_{iv} - E_{fu})$$

where P_{iv} is the Boltzmann distribution function of the initial state, H' is the interaction between two different Born–Oppenheimer states, and it contains two contributions as follows:

$$\hat{H}'\Psi_{iv} = \hat{H}^{BO}\Phi_i(r;\ Q)\Theta_v(Q) + \hat{H}^{SO}\Phi_i(r;\ Q)\Theta_v(Q)$$

where $\hat{H}^{BO}$ denotes the nonadiabatic coupling, and $\hat{H}^{SO}$ is the spin–orbit coupling. When the small term $\partial^2\Phi_i/\partial Q_{fl}^2$ is neglected, the first term reads:

$$\begin{aligned}&\langle\Phi_f\Theta_{fu}|\hat{H}^{BO}|\Phi_i\Theta_{iv}\rangle\\ &= -\hbar^2\sum_l\langle\Phi_f\Theta_{fu}|\frac{\partial\Phi_i}{\partial Q_{fl}}\frac{\partial\Theta_{iv}}{\partial Q_{fl}}\rangle\\ &= \sum_l\langle\Phi_f\Theta_{fu}|(\hat{P}_{fl}\Phi_i)(\hat{P}_{fl}\Theta_{iv})\rangle\rangle\end{aligned}$$

In the equation above, l is the index of the normal mode, and $\hat{P}_{fl}$ is the normal mode momentum operator of the lth normal mode in the final electronic state. So the internal conversion rate constant between two electronic states with same spin manifold can be written as

$$K_{IC} = \frac{2\pi}{\hbar}\sum_{kl} R_{kl}Z_i^{-1}\sum_{v,u} e^{-\beta E_{iv}}\langle\Theta_{fu}|\hat{P}_{fk}|\Theta_{iv}\rangle\langle\Theta_{iv}|\hat{P}_{fl}|\Theta_{fu}\rangle\delta(E_{iv} - E_{fu})$$

Here $R_{kl} = \langle\Phi_f|\hat{P}_{fk}|\Phi_i\rangle\langle\Phi_i|\hat{P}_{fl}|\Phi_f\rangle$ is the nonadiabatic electronic coupling. Further, the equation can be written as follows by applying the Fourier transform of the delta function:

$$K_{IC} = \sum_{kl}\frac{1}{\hbar^2}R_{kl}\int_{-\infty}^{\infty} dt[e^{iw_{if}t}Z_i^{-1}\rho_{IC}(t,\ T)]$$

Similarly, the intersystem crossing rate constant between two electronic states with different spin states can be written as

$$K_{ISC} = \frac{1}{\hbar^2}\langle\Phi_f|\hat{H}^{SO}|\Phi_i\rangle\int_{-\infty}^{\infty} dt[e^{iw_{if}t}Z_i^{-1}\rho_{ISC}(t,\ T)]$$

Both the methodology and application of this formalism can be found in Peng's and Shuai's work.[19−21]

In this article, a QM/MM method is used to study the electroluminescent properties of the TPA-AC molecules by considering the effect of the environment. The QM/MM model is shown in Figure 1b, and the detailed packing structure is shown in Figure 1c. The initial structure is obtained from the crystal structure detected experimentally.[15] Our QM/MM calculation is realized with the ONIOM method in *Gaussian 09* program.[22] The model consists two "layers"; the centered molecule is treated as a high layer and calculated by quantum mechanical method. The surrounding molecules are treated as low layer and computed by molecular mechanics with UFF forces field. Besides, the electronic embedding scheme is adopted in the ONIOM calculation.[23] Specifically, in the QM calculation, the ground-state (S0) optimization is performed based on density functional theory (DFT) with PBE0 functional and 6-311G(d) basis set, which has been proven to be effective to study the electronic structures of the organic molecules.[17] As for the first singlet excited state (S1) and the first and second triplet excited states (T1 and T2), the optimization of geometries and excitation energy calculations of the molecule are performed at the time-dependent density functional theory (TD-DFT) at PBE0/6-311G(d) level. Note that the "frozen optimization" is assumed in the optimization, which means that the surrounding molecules are frozen and that only the centered molecule is optimized. To obtain the frequencies of S0, S1, T1, and T2, the calculations are performed by DFT or TD-DFT at the same computational level, where the background charge is used to simulate the influence of the surrounding molecules.

To calculate the nonradiative rate, the reorganization energy is needed. There are two methods to obtain the reorganization energy. One is the adiabatic potential energy surface method (AP), and the other is the normal-mode analysis method (NM). For comparison, both the AP and NM methods are used here. In the AP method, the total reorganization energy, which corresponds to the Stokes shift in experiment, can be expressed as the sum of λ_{gs} and λ_{es} (shown in Figure 2). λ_{gs} and λ_{es} are the reorganization energies of the ground state S0 and the first excited state S1, respectively. E_{ab} and E_{em} are the absorption and emission energies. Moreover, the reorganization energy can also be expressed as a summation of the contributions from NM relaxation as in the harmonic oscillator approximation:

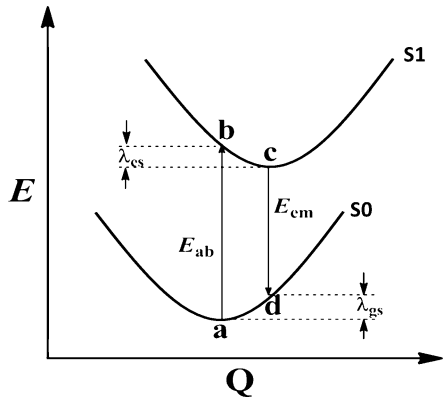

Figure 2. Schematic representation of the adiabatic potential energy surfaces for S0 and S1.

$$\lambda_{gs} = \sum_{j\in gs}\lambda_j = \sum_{j\in gs}\hbar w_j \mathrm{HR}_j$$

$$\lambda_{es} = \sum_{j\in es}\lambda_j = \sum_{j\in es}\hbar w_j \mathrm{HR}_j$$

$$\mathrm{HR}_j = \frac{w_j D_j^2}{2\hbar}$$

DOI: 10.1021/acs.jpca.6b09852
J. Phys. Chem. A 2016, 120, 9422−9430

Table 1. Selected Dihedral Angles (θ1, θ2, θ3, and θ4, deg) and Bond Lengths (B1 and B2, Å) Marked in Figure 1a Are Listed for S0, S1, and T2 States in the Gas Phase and Solid Phase, Respectively

	gas phase			solid phase		
	S0	S1	T2	S0	S1	T2
θ1	66.9	59.0	52.2	56.4	56.3	52.6
θ2	113.5	110.8	115.1	119.9	116.6	119.4
θ3	65.8	69.6	64.9	70.7	68.2	66.9
θ4	108.9	120.3	116.2	115.3	118.5	117.1
B1	1.482	1.472	1.461	1.480	1.472	1.462
B2	1.406	1.422	1.399	1.409	1.418	1.401

In the equation above, HR_j is the Huang−Rhys (HR) factor for the jth mode, and D_j represents the displacement for the mode j between the equilibrium geometries of S0 and S1. This can be realized in the DUSHIN program.[24]

On the basis of the calculation above, we calculate the nonradiative decay rate between S1 and S0 as well as the intersystem crossing rate from S1 to T2 and the reverse intersystem crossing rate from T2 to S1 by using the multimode coupled thermal vibration correlation function (TVCF) formalism realized in Molecular Materials Property Prediction Package (MOMAP),[25] which shows superiority in describing and predicting optical properties of polyatomic molecules.[26] For comparison, the photophysical properties and electroluminescence processes of TPA-AC in gas phase are also investigated with the same QM methods as performed in the solid state in this paper.

3. RESULTS AND DISCUSSION

3.1. Molecular Geometric Structure. For most D−A-type molecules, the excited states are often charge-transfer (CT) states. Some publications have shown that TD-DFT with nonhybrid functional always underestimates transition energies for CT states due to the neglecting of long-range Columbic attraction between the separated electrons and holes, while time-dependent Hartree−Fock (TD-HF) usually suffers from the so-called electron correlation problem, and it may overestimate transition energies.[27] Therefore, it is necessary to find an appropriate method to describe the excited states of D−A-type molecules. It is found that the excited-state calculation is largely dependent on the percentage of HF exchange incorporated within the functionals (HF%) for different molecules, and three new calculation methods were proposed and well-applied recently: the optimal Hartree−Fock (OHF) method, LC-wPBE method, and LC-BLYP method.[28−30] In this study, we calculate the absorption and emission wavelengths of S1 state by different functionals with different HF%. Besides, the Stokes shift and the vertical excitation energy of S1 and T1 as well as their vertical energy gap are listed in Table S1. Note that all the data in Table S1 is calculated in the gas phase. It is found that the absorption and emission wavelengths of the S1 state decreases with the increase of the HF%. Comparing with the experimental values (401/500 nm),[15] the absorption and emission wavelengths calculated with the MPW3LYP (439.6 nm/501.4 nm) and PBE0 (424.1 nm/477.3 nm) functionals show better agreement. Because of the unsuitability of MPW3LYP in the ONIOM method, the following calculation is performed with the PBE0 functional.

For convenience, some geometric parameters (marked in Figure 1a) for the S0, S1, and T2 states in both gas phase and solid state are listed in Table 1. Comparing these data for S0, S1, and T2 in gas phase, we can see that θ1 and θ4 change by ∼8° and 11° from S0 to S1, and the bond lengths of B1 and B2 change by ∼0.01 and 0.02 Å from S0 to S1 and T2, respectively. While in solid state, the dihedral angles of the molecule involved in S0, S1, and T2 only have a little difference, which indicates a minor geometry changes when the molecule transits from S0 to S1 and T2 in solid state than that in gas phase. This deviation should come from the influence of the surrounding molecules, which may restrict the movement of the atoms in the central molecule. Besides, the calculated θ1 is 56.4° in the solid phase, which is corresponding well with the crystal data (58°), which also confirms the reliability of the PBE0 functional and the ONIOM method used in the simulation. The different geometric change involved in the transition in solid state and in gas phase will be shown to have close relationship with the photophysical properties.

3.2. Excited-State Property and Energy Gap. The excited-state properties play an important role in determining the dynamics of excited states. The natural transition orbital (NTO) analysis for S1, T1, and T2 in gas phase and solid state are performed, and corresponding landscapes are shown in Figure 3a,b, respectively. It can be seen that the T1 state is a typical LE state in both gas phase and solid state. From Figure 3a, an obvious overlap, instead of absolute separation in pure CT state or complete overlap in pure LE state, can be found for S1 and T2 states in the gas phase. It is defined as a hybridized local and charge transfer (HLCT) excited state.[15] The HLCT state possesses both the property of an LE state, which contributes to a high-efficiency radiative rate due to its large orbital overlap, and a CT state, which is responsible for the full exciton utilization. Thus, the HLCT state is an effective pathway to obtain the high-efficiency CT-character luminescence. Specifically, for S1 and T2 states, the middle benzene ring between acridine and *N*-phenylaniline unit provides a meeting place for the highest occupied NTO and the lowest unoccupied NTO. Because of the large overlap from the LE contribution, the HLCT radiation becomes allowed and efficient; this is confirmed from the large oscillator strength and fluorescent rate of the S1 state (see Table 3). Besides, a more significant overlap can be found in the middle benzene ring for S1 in the solid state (Figure 3b), which may induce a faster fluorescent rate in the solid state.

The energy levels of the vertical and adiabatic excitation energy of the molecule calculated in gas phase and solid state are shown in Figure 4. It can be found that the energy levels of the molecule calculated in the gas phase are quite similar to those calculated in the solid state. Comparing Figure 4a,b, we can see that the absorption energy of S1 is bigger in gas phase than that in solid state, which means a red shift will be found in the solid state. From Figure 4d, we can see that the adiabatic energy levels of T2 and T3 are degenerate. The energy gap between T2 (T3) and T1 is as large as 1.78 eV, which will induce slow internal conversion from T2 (T3) to T1. In addition, the energy gap between T2

DOI: 10.1021/acs.jpca.6b09852
J. Phys. Chem. A 2016, 120, 9422−9430

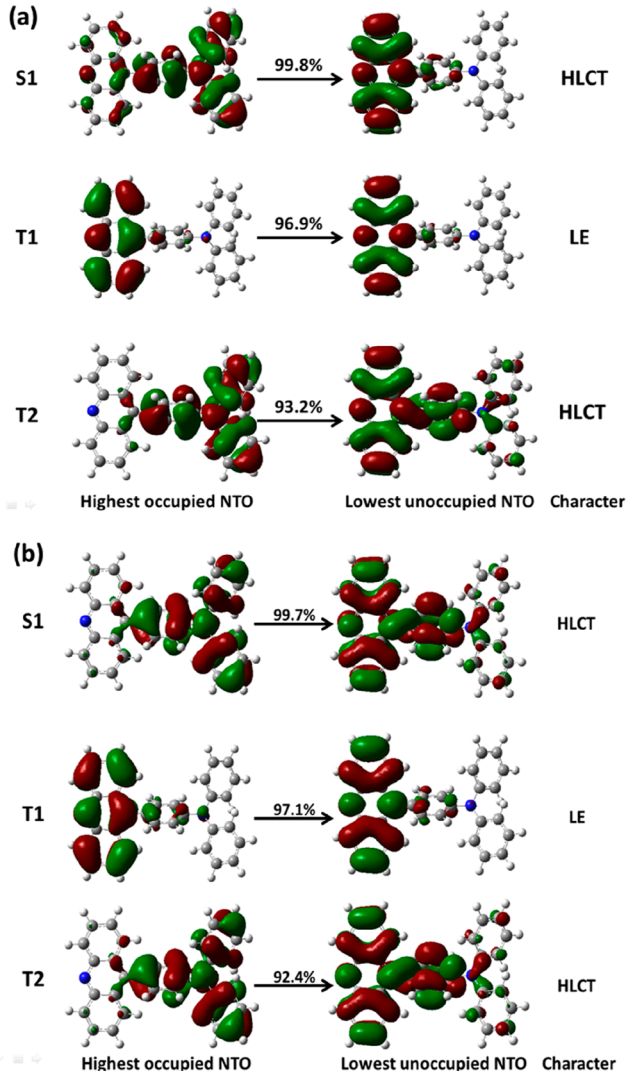

Figure 3. NTO character of selected excited states in gas phase (a) and in solid state (b).

(T3) to S1 is only 0.13 eV, which can efficiently help the up-conversion from the T2 (T3) state to the S1 state. Our results calculated in solid state have good agreement with the results of Ma's group, and they call the up-conversion process in higher excited states (not T1) the hot-exciton mechanism,[15] which is different from the TADF molecules proposed by Adachi's group, which involves the up-conversion from the T1 state to the S1 state.

3.3. Reorganization Energy and Huang–Rhys Factor. The reorganization energies calculated with both AP and NM methods are summarized in Table 2. It can be found that the reorganization energies obtained with two methods are consistent with each other, which indicates that the displaced harmonic oscillator approximation is reasonable both in gas phase and solid state. In addition the reorganization energy calculated in the solid state is 257 meV, which is much smaller than that calculated in gas phase (322 meV). For more details, we analyze the HR factor of each normal mode, which is an important parameter in measuring the extent of the electron-vibration coupling. The HR factors for S1 in the gas phase and solid state are shown in Figure 5a,b respectively. Comparing these HR factors, two distinct features can be found: (I) HR factors of TPA-AC calculated in the solid state are over 50 times smaller than that calculated in gas phase. (II) Vibration modes with large HR factors (>0.4) all appear in the low-frequency region such as 11.9 cm^{-1} (HR = 13.3) and 40.5 cm^{-1} (HR = 0.48) in the gas phase, and no HR factor is larger than 0.4 in the solid state. The two features indicate that the vibration of the molecules will be restricted to some extent in the real device, especially for the vibration modes with low frequencies. From the inset of Figure 5, we find that these vibration modes with large HR factors in the gas phase are the out-of-plane twisting motion of the acridine unit, which can induce the change of the dihedral angle $\theta 1$. From Table 1, we find that the angle $\theta 1$ has different changes when the molecule is pumped to excited states in gas phase and solid state. It should be induced by the suppression of the twisting motion of the acridine unit in the solid state.

The reorganization energy (λ_i) of every vibration mode of TPA-AC both in gas phase and solid state are shown in Figure 5c,d. The main difference between Figure 5c,d is the reduction of reorganization energy of the vibration modes with low frequencies. The contribution of all the low-frequency modes (<200 cm^{-1}) to the total reorganization energy is ~65 meV in the gas phase, while it decreases to 14 meV in the solid state. Consequently, the difference of the total reorganization energy in gas phase and solid state mainly comes from the contribution of the vibration modes with low frequencies.

To better clarify the relationship between molecular geometry variation and the reorganization energy, we decompose the reorganization energy into the contribution of bond lengths, bond angles, and dihedral angles both in gas phase and in solid state (shown in Figure S1a,b). It can be found that most of the reorganization energy comes from the relaxation of the bond lengths both in gas phase (57%) and solid state (68%). It also indicates that the contribution of the dihedral angle to the reorganization energy is ~76 meV in the gas phase, while it is only 26 meV in the solid state. This is the main reason for the reduction of the reorganization energy in solid state. It also confirms that suppression of the vibration of atoms related to the dihedral angles will be helpful to deduce the reorganization energy.

3.4. Dynamics of Several Low-Lying Excited States. The spin–orbit coupling constants (with the unit of cm^{-1}) between S1 and three lowest triplet excited states calculated both in gas phase and solid state are listed in Table S2. It can be found that the spin–orbit coupling constants are all quite small both in gas phase and solid state, and the difference between the values in two phases is also quite little. The radiative (K_r) and internal conversion (K_{IC}) rates from S1 to S0 as well as ISC (K_{ISC}) and RISC (K_{RISC}) rates between selected singlet and triplet states both in gas phase and solid state are summarized in Table 3. It is found that the radiative decay rate K_r is slightly increased in the solid state; this may be due to the enlarged overlap in the middle benzene ring between acridine and *N*-phenylaniline unit for S1 state in solid state. The nonradiative rate of S1 calculated in solid state is ~3 orders of magnitude smaller than that calculated in gas phase. This is not due to the calculation error but the suppression of the vibration in the solid state, which can significantly reduce the reorganization energy. To confirm the reliability of the internal conversion rate in our calculation, we plot the log K_{IC} (ΔE(eV)) parabola in Figure 6. No vibrational feature is found in both lines, which indicates the accuracy of the calculated K_{IC}. Besides, our calculation results are also consistent with the experimental results.

Moreover, the ISC and RISC rates between S1 and T2 are enhanced in the solid state, especially the RISC rate, which is

DOI: 10.1021/acs.jpca.6b09852
J. Phys. Chem. A 2016, 120, 9422–9430

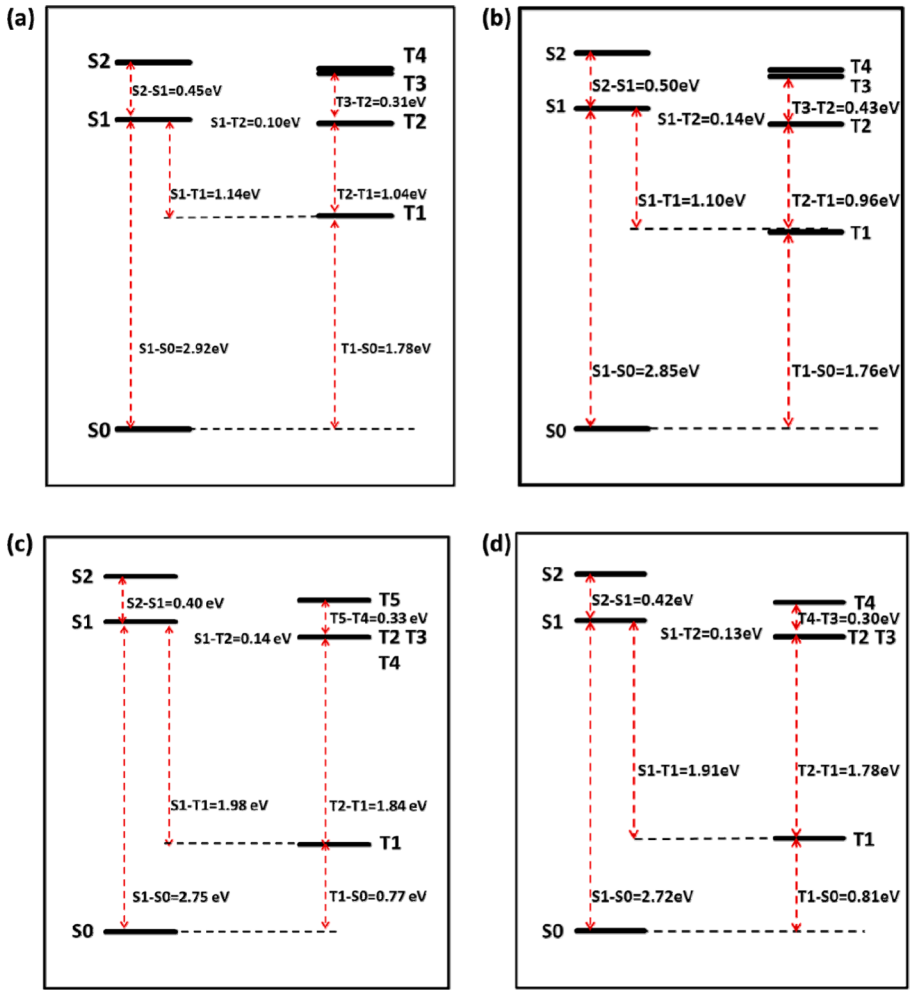

Figure 4. Energy landscape of vertical excitation for TPA-AC in gas phase (a) and in solid state (b). The energy landscape of adiabatic energy for TPA-AC in gas phase (c) and in solid state (d).

Table 2. Reorganization Energies Obtained by AP and NM Methods Both in Gas Phase and Solid Phase

	gas phase		solid state	
	AP	NM	AP	NM
λ_{gs}(meV)	160	156	129	127
λ_{es}(meV)	166	176	131	130
λ_{total}(meV)	326	332	260	257

mainly due to the decreased S1−T2 energy gap and increased spin−orbit coupling constant in the solid state. In addition, the ISC rates between the S1 and T3 as well as T4 are as high as 1×10^5 s^{-1}. Comparing the ISC and RISC rates between S1 and T3, we can see that the ISC rate calculated in solid state is a little smaller than that calculated in gas phase, while the RISC rate in the solid state become 31 times larger than that in the gas phase. The RISC rate from T2 to S1 in solid state increases 25 times more than that in gas phase. Because of the degeneration of the triplet excited states, we define the effective ISC and RISC rate between S1 and triplet excited stats as

$$K_{ISC} = \frac{K^2_{S1-T2} + K^2_{S1-T3}}{K_{S1-T2} + K_{S1-T3}}$$

$$K_{RISC} = \frac{K^2_{T2-S1} + K^2_{T3-S1}}{K_{T2-S1} + K_{T3-S1}}$$

On the basis of the formula above, we obtain the effective ISC and RISC rate between S1 and T2 (T3) as 3.30×10^5 s^{-1} and 1.51×10^4 s^{-1}, respectively, in solid state. It can also be seen that the ISC rate and the RISC rate between S1 and T1 are all quite small, which is owing to the large energy gap involved. It also makes the T1−S1 up-conversion impossible.

On the basis of the adiabatic energy levels of the molecule calculated in solid state (Figure 4) and the dynamics of excited states, the hot-exciton mechanism is confirmed (as illustrated in Figure 7). That means the triplet excitons are up-converted to the singlet excitons not from the T1 state but from the degenerate energy levels T2 and T3. Our result is a little different from Ma' s results,[15] where they found that only T2 is up-converted to S1. This deviation should come from the environment effect. Different from the TADF mechanism, the realization of the hot-exciton mechanism requires three conditions. One is that the energy gap between the high-lying triplet state (such as T2) and T1 is large enough (larger than 1 eV), which makes the internal conversion from high-lying triplet state to T1 impossible. The other is that the high-lying triplet state is close to S1 in energy, and the last one is that the fluorescent rate should be large

DOI: 10.1021/acs.jpca.6b09852
J. Phys. Chem. A 2016, 120, 9422−9430

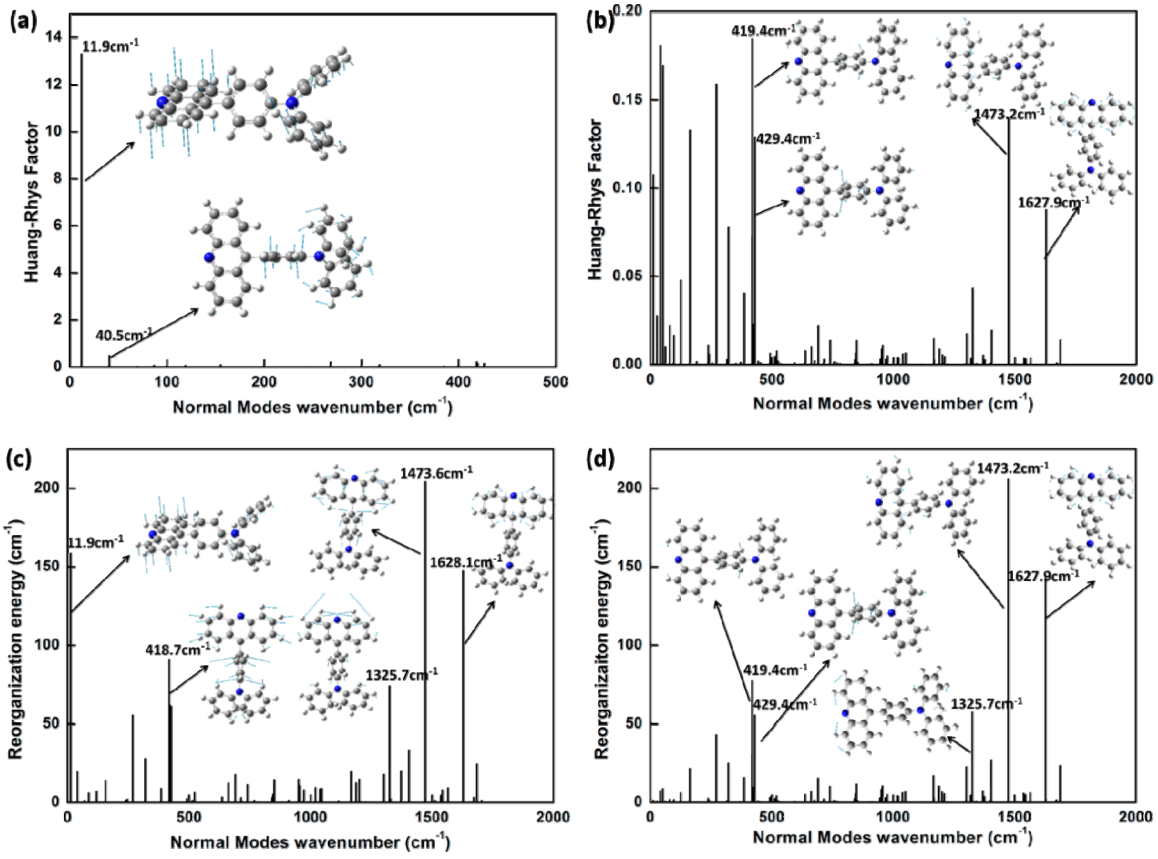

Figure 5. Calculated HR factors of TPA-AC in the gas phase (a) and solid state (b) as well as the reorganization energies in gas phase (c) and solid state (d). (inset) The corresponding vibration modes.

Table 3. Rate Constants of Radiative and Nonradiative as well as ISC and RISC Calculated Both in Gas Phase and Solid Phase

	K_r (s^{-1}) (S1→S0)	K_{IC} (s^{-1}) (S1→S0)	K_{ISC} (s^{-1}) (S1→T1)	K_{RISC} (s^{-1}) (T1→S1)	K_{ISC} (s^{-1}) (S1→T2)	K_{RISC} (s^{-1}) (T2→S1)	K_{ISC} (s^{-1}) (S1→T3)	K_{RISC} (s^{-1}) (T3→S1)	K_{ISC} (s^{-1}) (S1→T4)	K_{RISC} (s^{-1}) (T4→S1)
gas	4.95×10^7	9.67×10^{10}	1.54×10^3	0	1.53×10^4	1.73×10^2	8.53×10^5	5.53×10^2	3.50×10^5	6.93×10^2
solid	6.46×10^7	3.13×10^7	1.00×10^2	5.7×10^1	3.17×10^4	4.57×10^3	3.57×10^5	1.78×10^4		

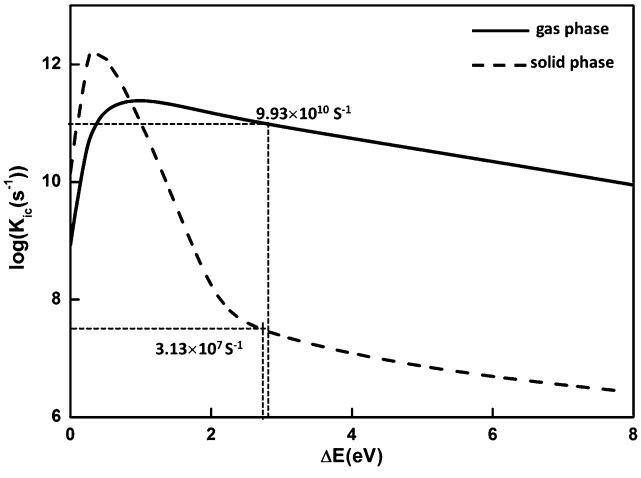

Figure 6. Internal conversion rate K_{ic} versus the energy gap ΔE in both gas and solid phase for TPA-AC, the vertical line indicates the position of the adiabatic energy gap between S1 and S0.

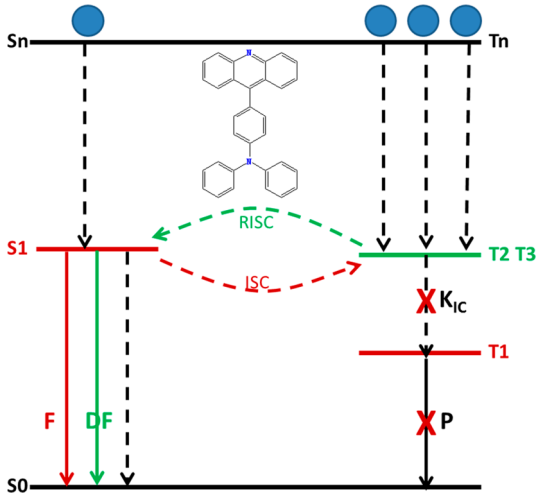

Figure 7. Scheme of the Electroluminescence Process for TPA-AC.

enough (at least larger than the ISC rate). Only when all three conditions are satisfied, the hot-exciton mechanism can happen.

4. CONCLUSION

To summarize, the excited-state dynamics of the TPA-AC molecule in solid state is investigated based on the QM/MM

DOI: 10.1021/acs.jpca.6b09852
J. Phys. Chem. A 2016, 120, 9422−9430

study. In solid state, the nonradiative rate from S1 to S0 is smaller than the fluorescent rate, which is in agreement with the experimental results, while it is ∼3 orders of magnitude larger than the fluorescent rate calculated in gas phase. By performing the vibrational analysis of the HR factor and the reorganization energy, we find that the reorganization energy is significantly reduced in solid state due to the suppression of the vibrations with low frequencies, which mostly involve dihedral angles. This is consistent with the geometry change that shows a smaller dihedral angle change between S1 and S0 in solid state than that in gas phase. Although calculations in both phases confirm the HLCT property of the S1 state, more LE component can be found for S1 in the solid state. This is also one important factor that makes a larger fluorescent rate of the molecule in solid state than that in gas phase. In addition, combing the dynamics of several low-lying excited states with the energy structure of the TPA-AC molecule calculated in solid state further illustrates the hot-exciton mechanism proposed by Ma's group. All of the above investigations demonstrate the importance of molecular interaction for theoretical simulation of the working principle of OLEDs.

■ ASSOCIATED CONTENT

Supporting Information

The Supporting Information is available free of charge on the ACS Publications website at DOI: 10.1021/acs.jpca.6b09852.

Spin-orbit coupling constants, contributions to reorganization energy from bond length and angles, HF% of functionals (PDF)

■ AUTHOR INFORMATION

Corresponding Authors

*E-mail: ckwang@sdnu.edu.cn. (C.-K.Wang.)
*E-mail: linll@sdnu.edu.cn. (L.L.Lin)

Notes

The authors declare no competing financial interest.

■ ACKNOWLEDGMENTS

This work is supported by the National Natural Science Foundation of China (Grant Nos. 11374195 and 21403133). Thanks to the supporting of Taishan Scholar Project of Shandong Province and the Scientific Research Foundation of Shandong Normal Univ. Thanks to the supporting of the Promotive Research Fund for Excellent Young and Middle-aged Scientists of Shandong Province (Grant No. BS2014CL001) and the General Financial Grant from the China Postdoctoral Science Foundation (Grant No. 2014M560571). Great thanks to Prof. Y. Luo and T. Lu for their helpful suggestions and discussions in the detail calculations. Thanks to Prof. B. Yang for providing the crystal data, and thanks to Prof. Y. Niu for the usage of MOMAP.

■ REFERENCES

(1) Tang, C. W.; VanSlyke, S. A. Organic Electroluminescent Diodes. *Appl. Phys. Lett.* **1987**, *51*, 913−915.

(2) Forrest, S. R.; O'Brien, D.; You, Y.; Shoustikov, A.; Sibley, S.; Thompson, M.; Baldo, M. A. Highly Efficient Phosphorescent Emission from Organic Electroluminescent Devices. *Nature* **1998**, *395*, 151−154.

(3) Vahtras, O.; Ågren, H.; Jorgensen, P.; Jensen, H. J. r. A.; Helgaker, T.; Olsen, J. Multiconfigurational Quadratic Response Functions for Singlet and Triplet Perturbations: The Phosphorescence Lifetime of Formaldehyde. *J. Chem. Phys.* **1992**, *97*, 9178−9187.

(4) Adachi, C.; Baldo, M. A.; Thompson, M. E.; Forrest, S. R. Nearly 100% Internal Phosphorescence Efficiency in an Organic Light-Emitting Device. *J. Appl. Phys.* **2001**, *90*, 5048−5051.

(5) Cherpak, V.; Stakhira, P.; Minaev, B.; Baryshnikov, G.; Stromylo, E.; Helzhynskyy, I.; Chapran, M.; Volyniuk, D.; Hotra, Z.; Dabuliene, A.; et al. Mixing of Phosphorescent and Exciplex Emission in Efficient Organic Electroluminescent Devices. *ACS Appl. Mater. Interfaces* **2015**, *7*, 1219−1225.

(6) Uoyama, H.; Goushi, K.; Shizu, K.; Nomura, H.; Adachi, C. Highly Efficient Organic Light-Emitting Diodes from Delayed Fluorescence. *Nature* **2012**, *492*, 234−238.

(7) Zhang, Q. S.; Li, J.; Shizu, K.; Huang, S. P.; Hirata, S.; Miyazaki, H.; Adachi, C. Design of Efficient Thermally Activated Delayed Fluorescence Materials for Pure Blue Organic Light Emitting Diodes. *J. Am. Chem. Soc.* **2012**, *134*, 14706−14709.

(8) Lee, J.; Shizu, K.; Tanaka, H.; Nomura, H.; Yasuda, T.; Adachi, C. Oxadiazole-and Triazole-Based Highly-Efficient Thermally Activated Delayed Fluorescence Emitters for Organic Light-Emitting Diodes. *J. Mater. Chem. C* **2013**, *1*, 4599−4604.

(9) Li, J.; Nakagawa, T.; MacDonald, J.; Zhang, Q. S.; Nomura, H.; Miyazaki, H.; Adachi, C. Highly Efficient Organic Light-Emitting Diode Based on a Hidden Thermally Activated Delayed Fluorescence Channel in a Heptazine Derivative. *Adv. Mater.* **2013**, *25*, 3319−3323.

(10) Tanaka, H.; Shizu, K.; Nakanotani, H.; Adachi, C. Dual Intramolecular Charge-Transfer Fluorescence Derived from a Phenothiazine-Triphenyltriazine Derivative. *J. Phys. Chem. C* **2014**, *118*, 15985−15994.

(11) Nakagawa, T.; Ku, S.; Wong, K.; Adachi, C. Electroluminescence Based on Thermally Activated Delayed Fluorescence Generated by a Spirobifluorene Donor−Acceptor Structure. *Chem. Commun.* **2012**, *48*, 9580−9582.

(12) Zhang, Q.; Kuwabara, H.; Potscavage, W. J., Jr.; Huang, S.; Hatae, Y.; Shibata, T.; Adachi, C. Anthraquinone-Based Intramolecular Charge-Transfer Compounds: Computational Molecular Design, Thermally Activated Delayed Fluorescence, and Highly Efficient Red Electroluminescence. *J. Am. Chem. Soc.* **2014**, *136*, 18070−18081.

(13) Yao, L.; Yang, B.; Ma, Y. Progress in Next-Generation Organic Electroluminescent Materials: Material Design Beyond Exciton Statistics. *Sci. China: Chem.* **2014**, *57*, 335−345.

(14) Li, W.; Pan, Y.; Xiao, R.; Peng, Q.; Zhang, S.; Ma, D.; Li, F.; Shen, F.; Wang, Y.; Yang, B.; et al. Employing 100% Excitons in Oleds by Utilizing a Fluorescent Molecule with Hybridized Local and Charge-Transfer Excited State. *Adv. Funct. Mater.* **2014**, *24*, 1609−1614.

(15) Li, W.; Pan, Y.; Yao, L.; Liu, H.; Zhang, S.; Wang, C.; Shen, F.; Lu, P.; Yang, B.; Ma, Y. A Hybridized Local and Charge-Transfer Excited State for Highly Efficient Fluorescent Oleds: Molecular Design, Spectral Character, and Full Exciton Utilization. *Adv. Opt. Mater.* **2014**, *2*, 892−901.

(16) Bu, F.; Duan, R.; Xie, Y.; Yi, Y.; Peng, Q.; Hu, R.; Qin, A.; Zhao, Z.; Tang, B. Z. Unusual Aggregation-Induced Emission of a Coumarin Derivative as a Result of the Restriction of an Intramolecular Twisting Motion. *Angew. Chem., Int. Ed.* **2015**, *54*, 14492−14497.

(17) Zhang, T.; Peng, Q.; Quan, C.; Nie, H.; Niu, Y.; Xie, Y.; Zhao, Z.; Tang, B. Z.; Shuai, Z. Using the Isotope Effect to Probe an Aggregation Induced Emission Mechanism: Theoretical Prediction and Experimental Validation. *Chemical Science* **2016**, *7*, 5573−5580.

(18) McCumber, D. E. Einstein Relations Connecting Broadband Emission and Absorption Spectra. *Phys. Rev.* **1964**, *136*, A954−A957.

(19) Niu, Y.; Peng, Q.; Deng, C.; Gao, X.; Shuai, Z. Theory of Excited State Decays and Optical Spectra: Application to Polyatomic Molecules. *J. Phys. Chem. A* **2010**, *114*, 7817−7831.

(20) Peng, Q.; Niu, Y. L.; Shi, Q. H.; Gao, X.; Shuai, Z. G. Correlation Function Formalism for Triplet Excited State Decay: Combined Spin-Orbit and Nonadiabatic Couplings. *J. Chem. Theory Comput.* **2013**, *9*, 1132−1143.

(21) Shi, Q. H.; Peng, Q.; Sun, S. R.; Shuai, Z. G. Vibration Correlation Function Investigation on the Phosphorescence Quantum Efficiency and Spectrum for Blue Phosphorescent Ir(Iii) Complex. *Huaxue Xuebao* **2013**, *71*, 884.

DOI: 10.1021/acs.jpca.6b09852
J. Phys. Chem. A 2016, 120, 9422−9430

(22) Frisch, M. J.; Trucks, G. W.; Schlegel, H. B.; Scuseria, G. E.; Robb, M. A.; Cheeseman, J. R.; Scalmani, G.; Barone, V.; Mennucci, B.; Petersson, G. A.; et al. *Gaussian 09,* revision D.01; Gaussian Inc: Wallingford, CT, 2009.
(23) Morokuma, K.; Wang, Q.; Vreven, T. Performance Evaluation of the Three-Layer Oniom Method: Case Study for a Zwitterionic Peptide. *J. Chem. Theory Comput.* **2006**, *2*, 1317−1324.
(24) Reimers, J. R. A Practical Method for the Use of Curvilinear Coordinates in Calculations of Normal-Mode-Projected Displacements and Duschinsky Rotation Matrices for Large Molecules. *J. Chem. Phys.* **2001**, *115*, 9103−9109.
(25) Niu, Y.; Peng, Q.; Shuai, Z. Promoting-Mode Free Formalism for Excited State Radiationless Decay Process with Duschinsky Rotation Effect. *Sci. China, Ser. B: Chem.* **2008**, *51*, 1153−1158.
(26) Zhang, T.; Ma, H. L.; Niu, Y. L.; Li, W. Q.; Wang, D.; Peng, Q.; Shuai, Z. G.; Liang, W. Z. Spectroscopic Signature of the Aggregation-Induced Emission Phenomena Caused by Restricted Nonradiative Decay: A Theoretical Proposal. *J. Phys. Chem. C* **2015**, *119*, 5040−5047.
(27) Dreuw, A.; Head-Gordon, M. Failure of Time-Dependent Density Functional Theory for Long-Range Charge-Transfer Excited States: The Zincbacteriochlorin−Bacteriochlorin and Bacteriochlorophyll−Spheroidene Complexes. *J. Am. Chem. Soc.* **2004**, *126*, 4007−4016.
(28) Huang, S. P.; Zhang, Q. S.; Shiota, Y.; Nakagawa, T.; Kuwabara, K.; Yoshizawa, K.; Adachi, C. Computational Prediction for Singlet- and Triplet-Transition Energies of Charge-Transfer Compounds. *J. Chem. Theory Comput.* **2013**, *9*, 3872−3877.
(29) Penfold, T. J. On Predicting the Excited-State Properties of Thermally Activated Delayed Fluorescence Emitters. *J. Phys. Chem. C* **2015**, *119*, 13535−13544.
(30) Sun, H.; Zhong, C.; Brédas, J.-L. Reliable Prediction with Tuned Range-Separated Functionals of the Singlet−Triplet Gap in Organic Emitters for Thermally Activated Delayed Fluorescence. *J. Chem. Theory Comput.* **2015**, *11*, 3851−3858.

DOI: 10.1021/acs.jpca.6b09852
J. Phys. Chem. A 2016, 120, 9422−9430